Performance Analysis of MOS-HEMT as a Biosensor: A Dielectric Modulation Approach

Ritu Poonia (pooniaritu247@gmail.com)
MNIT Jaipur: Malaviya National Institute of Technology https://orcid.org/0000-0002-7292-4080
Aasif Mohammad Bhat
MNIT Jaipur: Malaviya National Institute of Technology
C. Periasamy
MNIT Jaipur: Malaviya National Institute of Technology
Chitrakant Sahu
MNIT Jaipur: Malaviya National Institute of Technology

Research Article

Keywords: AlGaN/GaN High electron mobility transistor (HEMT) , Dielectric modulation , Interface charge , Threshold voltage sensitivtiy , Drain current sensitivity

Posted Date: October 22nd, 2021

DOI: https://doi.org/10.21203/rs.3.rs-1003011/v1

Silicon manuscript No.
(will be inserted by the editor)

Performance Analysis of MOS-HEMT as a Biosensor:A Dielectric Modulation Approach

Ritu Poonia · Aasif Mohammad Bhat · C. Periasamy · Chitrakant Sahu

Received: date / Accepted: date

Abstract In this work, we have reported the simulation study and electrical properties of MOS-HEMT with a cavity on the source side for bio-sensing applications. The effect of the neutral and charged biomolecules on the sensitivity and concentration of electrons is analyzed. The increase of dielectric observed drain current decreases and increases due to the rise of the positive charge of the biomolecules. The different cavity lengths are taken into consideration to analyze the performance of the device. The maximum threshold voltage sensitivity obtained for keratin is 26% and 51% for charged biomolecules at 500mm cavity length. The effect of the AlGaN barrier mole fraction on sensitivity was also studied and optimized. The maximum sensitivity obtained is 74.04% for charged biomolecules. The device shows high stability under high-temperature conditions. The MOS-HEMT structure is optimized and analyzed using the ATLAS Silvaco device simulation tool.

Keywords AlGaN/GaN High electron mobility transistor (HEMT) · Dielectric modulation · Interface charge · Threshold voltage sensitivtiy · Drain current sensitivity

1 Introduction

In recent years HEMT based biosensors have attracted researchers due to their quick response, simple detection, and bio compatibility [1]. High scalability, less area, higher sensitivity, low cost, and user-friendly make field-effect transistors prominent for bio-sensing applications. GaN-based materials have unique features which make them attractive for high RF applications. The dielectric modulated approach enables sensing of biomolecules in a Nano-gap/Nano-cavity region. Silicon-based devices are not chemically stable. They showed very low sensitivity towards biomolecules and are not compatible with high-temperature conditions due to their small band-gap compared to GaN. The polarization of AlGaN/AlN/GaN HEMT generates the electric field that pulls the surface state electrons to the empty conduction band (CB) states at the heterojunction, resulting in 2DEG formation [2]. The presence of high sheet charge density and mobility increases the sensitivity [3]. Various research has been done on HEMT based biosensor for pH detection [4][5][6][7], Immuno-detection using floating gate AlGaN HEMT[8],deoxyribonucleic acid (DNA)[9], Urea testing[10], Prostate-specific antigen testing[11][12], Monokine induced by interferon gamma[13], CerbB2 detection[14], CO and H_2 detection[3][15], C-reactive protein detection[16], troponin I testing[17][18] and carcinoembryonic antigen (CEA) detection respectively. To enhance the sensitivity of the proposed HEMTs device, various structures are also optimized like Circular gate HEMT, Double gate, Gateless devices, Nano-cavity under the gate region towards the drain side, and Nano-cavity at the source and drain both sides, respectively. The effect of half and fully filled cavity on sensitivity was also reported. In the previous reports, the effect of mole fraction on biomolecule sensitivity is not reported [19]. In this work, Gated MOS-HEMT is proposed to sense biological agents. The cavity on the source side is embedded for the first time using HEMT. The performance metrics of the device depends on threshold voltage sensitivity, drain current variation, and channel conductance variation. The de-

Department of Electronics and Communication Engineering
Malaviya National Institute of Technology Jaipur
Rajasthan-302017, India
E-mail: pooniaritu247@gmail.com

vice is capable of detecting both neutral and charged biomolecules. This paper presents a HEMT with a Nano-cavity that can be used for various bio sensing applications. The rest of the paper is organized as Section 2 presenting the HEMT device architecture and simulation parameters procedure. The results and discussions are reported in Section 3, which is later summarized as the conclusion.

2 Device Architecture and Simulation Parameters

The proposed device structure and enlarged cavity view in MOS-HEMT are shown in Fig.1(a) and (b), respectively. The device consists gate length = 1μm ,Oxide thickness (t_{ox}) = 10nm , source to gate length(L_{SG}) and gate to drain length(L_{GD}) is 1μm and 2μm respectively. The space between gate to drain (L_{GD}) is kept larger than the space between source to gate (L_{SG}) to increases the breakdown voltage of the device [20].

The cavity is designed towards the source side to improve the device on current (I_{ON}). $Al_xGa_{1-x}N$ thickness is kept as 25nm, the Buffer layer thickness is 3μm, AlN spacer layer thickness is 3nm and AlN nucleation layer thickness is 100nm. The AlN spacer reduces the Coulomb scattering of charge carriers at the interface and enhances the channel's carrier concentration. The nucleation layer is used to reduce lattice mismatch of GaN and the Substrate layer [21]. According to the proposed design cavity is considered here as a sensing area for biomolecules. The cavity length and height of the proposed devices are 500nm and 7nm, respectively. The mole fraction of the barrier layer considered is x=0.30. When we fill the cavity with biomolecules, a stern is formed, represented by SiO_2 over the gate oxide. Ti/Al/Ni/Au is used to make source/drain ohmic contact, and Ni/Au is used as a gate material [19]. Afterward, SiO_2 oxide is then etched to create the cavity of 500nm length and 7nm height on the source side below the gate region. Si_3N_4 will be used as a passivation layer over the exposed area of the device to prevent the device from other environmental effects. Sensing for both neutral and charged biomolecules is achieved with the proposed architecture. Only permittivity is associated with neutral biomolecules, whereas charged biomolecules are associated with both permittivity and charge. The AlGaN/GaN HEMT has high electron mobility and is then etched to create the cavity of 500nm length high saturation velocity due to high electron confinement at the heterojunction. The basic working principle of the GaN/AlGaN MOS-HEMT device is the modulation of polarization charge density at the heterojunction, as given in Equation (1) [22].

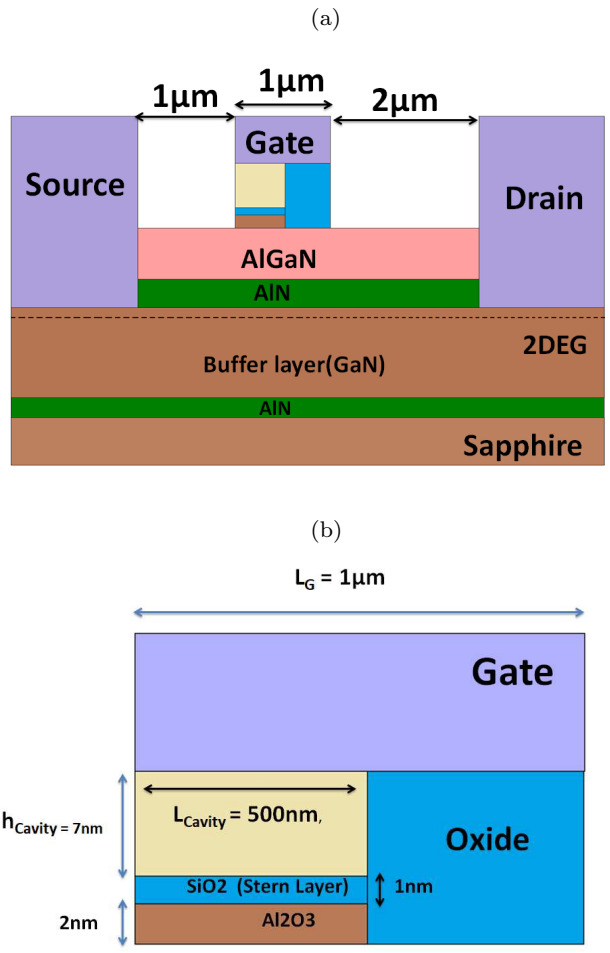

Fig. 1 (a) Schematic cross-sectional view of the AlGan/AlN/GaN based MOS-HEMT for Biosensing applications ,(b)Schematic cross-sectional view of Nano-cavity under the gate region.

$$Q_{Polar} = \frac{\sigma}{q} - \frac{\epsilon_{oxide}\epsilon_{AlGaN}}{Q^2 d_{AlGaN}} q\phi_{AlGaN}[q\phi_b + E_F - \delta E_c] \quad (1)$$

where ϵ_{oxide} oxide is the dielectric constant of oxide,ϵ_{AlGaN} is the dielectric constant and d_{AlGaN} is width of the barrier layer, respectively, $q\phi_b$ is the gate barrier height. The threshold voltage given in the below equation for a MOS-HEMT shows the dependence on the dielectric constant and thickness of oxide and barrier layer [9].

$$V_{th} = \frac{\phi_b}{Q} - \frac{\Delta E_C}{Q} - \frac{\phi_f}{Q} - \frac{qt_{oxide}}{\epsilon_{oxide}}\rho - \frac{Qt^2{}_{oxide}}{2\epsilon_{oxide}} n_{oxide} - Q\left(\frac{t_{oxide}}{\epsilon_{oxide}} + \frac{d_{AlGaN}}{\epsilon_{AlGaN}}\right) \quad (2)$$

where ρ is the charge density at the interface, δE_C is the conduction band offset ,ϕ_f Fermi level separation from conduction band of buffer layer and n_{oxide} is the average charge density of oxide. Q_{Polar} is the polarization charge density at hetero junction. Models used in the simulation analysis are Field-dependent drift velocity (FLDMOB), concentration-dependent mobility (CONMOB), Albrct.n, Shockley–Read–Hall (SRH), Polarization, and Calc. strain. The recombination effect is accounted for SRH, while the low field mobility effects accounted for albrct. n. The simulation models

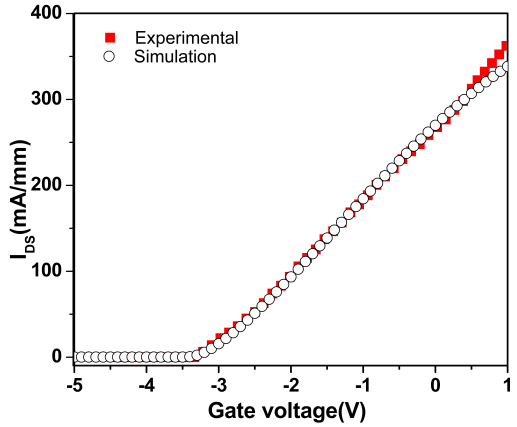

Fig. 2 Validation of methods and models with experimental results

and methods depict a good agreement with the experimentally measured response of [23], as shown in figure 2. The dimensions used for simulation are the same as experimental.

3 Results and Discussion

The sensitivity analysis is carried out for Neutral, negatively charged, and positively charged bio-molecules. The neutral biomolecules given in Table 1 are analyzed. The charged biomolecules are analyzed range from $3 \times 10^{12}/\text{cm}^2$ to $-5 \times 10^{12}/\text{cm}^2$, which includes the DNA charge ranges from $-1 \times 10^{12}/\text{cm}^2$ to $-1 \times 10^{11}/\text{cm}^2$[9]. The dielectric of air(K=1) is considered as reference to differentiate the change in device performance parameters after exposure to different biomolecules. To obtain the sensitivity of the devices for various biomolecule drain currents and the threshold voltage has been considered. The AlGaN/AlN/GaN MOS- HEMT shows a sheet charge density of $1.39 \times 10^{13}/cm^2$.

As depicted in Fig.(3), the channel potential drops as on the increase of dielectric of the cavity. The highest obtained channel potential is for urease. In the case of the charged biomolecules cavity is filled with dielectric

Table 1 Neutral biomolecules and their dielectric.

Bio molecule	Dielectric constant(K)
Air(ref)	1
Urease[24]	1.64
Streptavidin[10]	2.1
Biotin[25]	2.63
Glucose-Oxidase (Gox)[26]	3.46
Zein[27]	5
kertain[27][28][29]	8

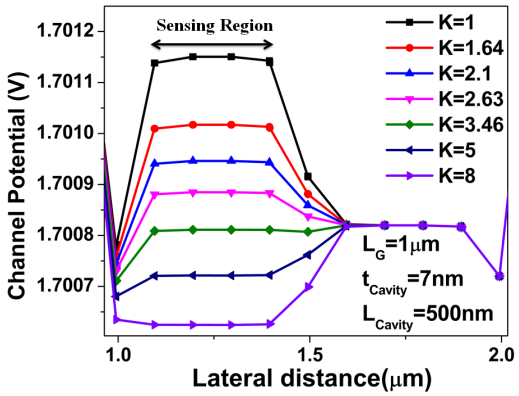

Fig. 3 Channel potenial of different neutral biomolecules in the gate region

constant K=2. The total capacitance of the device is the sum of the capacitance of four regions under the gate area. Capacitance for oxide and cavity gave by equations (1) and (2)

$$C_{Oxide} = \frac{\epsilon_{Oxide}}{t_{Oxide}} \tag{3}$$

$$C_{Bio} = \frac{\epsilon_{Bio}}{t_{Bio}} \tag{4}$$

$$C_{Al_2O_3} = \frac{\epsilon_{Al_2O_3}}{t_{Al_2O_3}} \tag{5}$$

$$C_{stern} = \frac{\epsilon_{stern}}{t_{stern}} \tag{6}$$

The capacitance of the cavity is defined by ,

$$C_{cavity} = (C_{bio}||C_{Al_2O_3}||C_{stern}) \tag{7}$$

The total effective capacitance is defined by,

$$C_{effect.} = C_{SiO_2} + C_{cavity} \tag{8}$$

Now the device total capacitance is defined as follows:

$$\frac{1}{C_{total}} = \frac{1}{C_{effect.}} + \frac{1}{C_{AlGaN}} \tag{9}$$

Where C_{AlGaN} is the capacitance of barrier layer that is defined as follows:

$$C_{AlGaN} = \frac{\epsilon_{AlGaN}}{t_{AlGaN}} \tag{10}$$

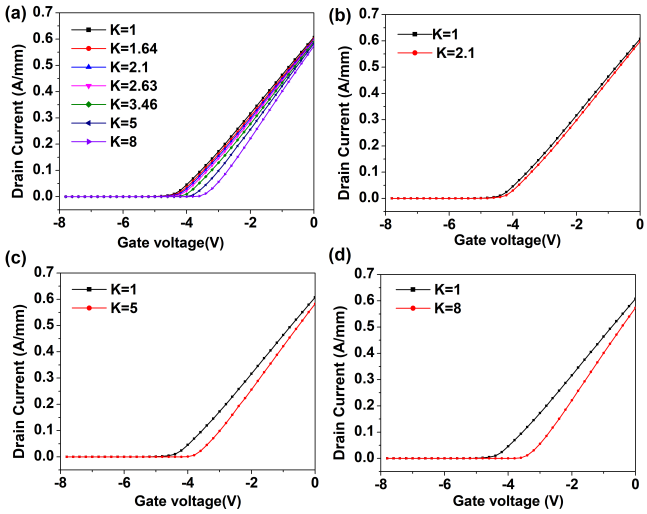

Fig. 4 Transfer characteristics for neutral biomolecules at V_{DS} = 5V for (a) all neutral biomolecules, (b) Streptavidin(k=2.1), (c) Zein(k=5) and (d) Kertain(k=8)

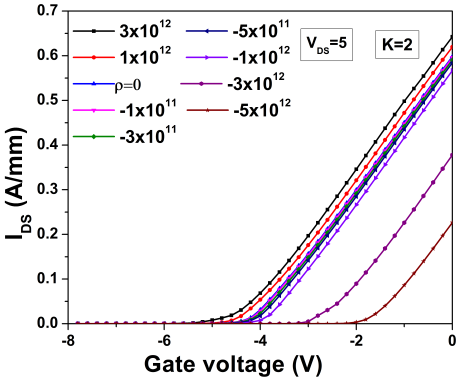

Fig. 5 Transfer characteristics for charged biomolecules at V_{DS} = 5V

Where the permittivity of AlGaN is calculated using the following equation;

$$\epsilon_{AlGaN} = -0.3 \times m + 10.4 \quad (11)$$

Where m(0.22,0.25,0.30) is the mole fraction of the barrier layer. t_{AlGaN} is the thickness of the AlGaN layer. To obtain the electrical characteristics in the presence of neutral biomolecules, we considered the dielectric constant of the cavity. The effect on the electrical characteristics of charged biomolecules is also analyzed.

Fig.4 (a) presents the transfer characteristics of the device for different neutral biomolecules with different dielectric values. Fig.4 (b-d) illustrates the variation in threshold voltage for Streptavidin, Zein, Keratin molecules w.r.t K=1. The maximum shift obtained is -3.67V for Keratin. The Threshold voltage shifts towards less negative value due to an increase in the dielectric of a biomolecule in the cavity. The effect of

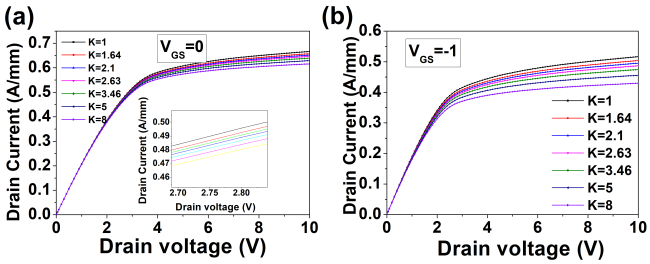

Fig. 6 Output characteristics of the device for neutral biomolecules

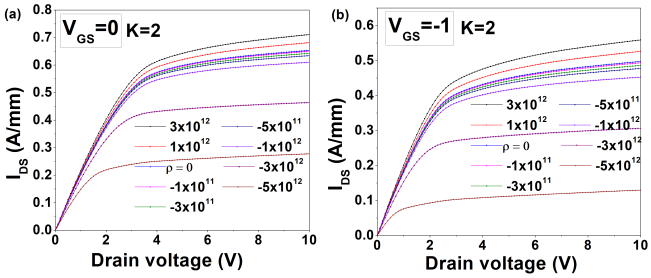

Fig. 7 Output characteristics of the device for charged biomolecules at (a) $V_{GS} = 0V$ and (b) $V_{GS} = -1V$

charge biomolecules on device characteristics are also analyzed in this work. Fig.5 represents the $I_{DS} - V_{GS}$ for charged molecules. The figure depicts that the increment of negative charge of the biomolecule decreases the drain current and increment of positive charge increases the drain current due to the depletion or enhancement of the channel carriers, respectively. The device output characteristics are shown in Fig.6 and 7, respectively for neutral and charged species. The device is biased at $V_{GS} = 0V$ and $V_{GS} = -1V$. The device is biased at $V_{GS} = -1V$ because of maximum transconductance at this gate voltage. As depicted in Fig.6 (a) and (b) the drain current will start decreasing on increasing of the dielectric. The more relative change in current, the more sensitivity will be. The maximum current observed for neutral molecules is 656mA/mm for urease. Fig.7 (a) and (b) presents the charged biomolecules output characteristics. The drain current increases when the biomolecule carries a positive charge. Applying positive charge on the interface will attract more electrons to the channel, whereas the increment of charge carriers will increase the current in the device.

In the case of a negative charge, the current will decrease due to the charge carriers' depletion. Fig.8 and 9 show the drain current variation induced by different biomolecules. In the case of neutral biomolecules, the maximum drain current variation obtained for keratin is 86.2mA/mm, whereas the minimum current variation is 12.4mA/mm for urease at $V_{GS} = -1V$. The maximum current obtained at $V_{GS} = 0V$ is 50.5mA/mm for keratin, whereas the minimum is 8.6mA/mm for urease. In

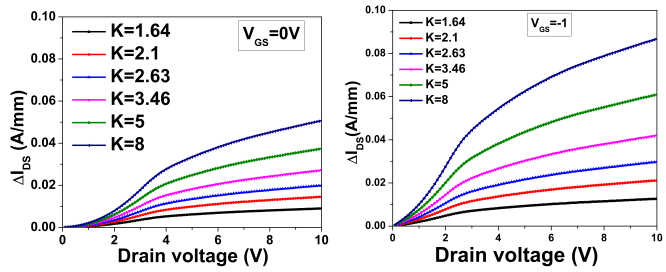

Fig. 8 Drain current variation for neutral biomolecules at (a) $V_{GS} = 0V$ and (b) $V_{GS} = -1V$

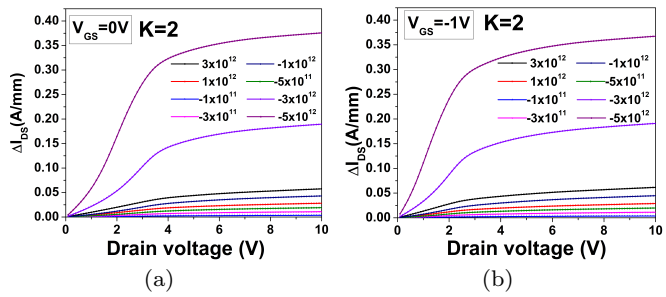

Fig. 9 Drain current variation for charged biomolecules at (a) $V_{GS} = 0V$ and (b) $V_{GS} = -1V$

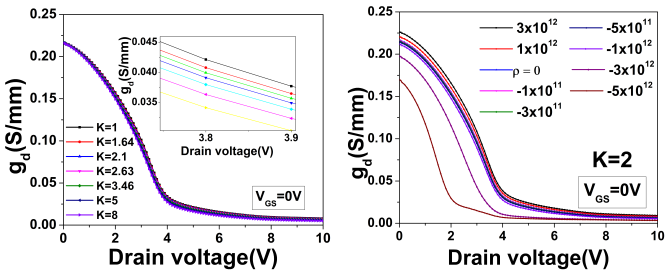

Fig. 10 Channel conductance at V_{GS}=0V for (a) neutral and (b) charged biomolecules

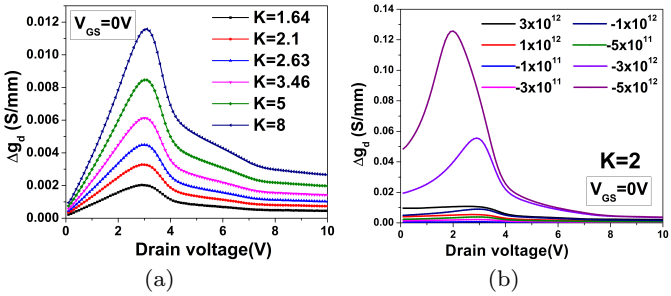

Fig. 11 Channel conductance variation at V_{GS}=0V for different (a) neutral and (b) charged biomolecules

the case of charged biomolecules, the more negative the charge more the relative change in current w.r.t $\rho = 0$. When the negative charge of the biomolecule increases at the interface the drain current reduces. The more positive charge means more current due to the enhancement of the carriers. The device is sensible for charge ranges from $3 \times 10^{12}/\text{cm}^2$ to $-5 \times 10^{12}/\text{cm}^2$. The maximum current measured is 710(mA/mm) at $3 \times 10^{12}/\text{cm}^2$ due to an increase in positive charge will increase the charge carrier concentration in the channel. The device is biased at $V_{GS} = 0V$. to observe the pure effect of neutral and charged species on the device. When a molecule consists of charges and dielectric, the device parameters are affected by both dielectric and charge density. To analyze the effect of DNA charge, varying its charge from $-1 \times 10^{12}/\text{cm}^2$[9] to $-1 \times 10^{11}/\text{cm}^2$[9].

As shown in Fig.9, the maximum current variation measured at $V_{GS} = -1V$ for $V_{GS} = -1V$ is 375.5mA/mm, whereas the minimum is 3.55mA/mm at $V_{GS} = -1V$ for$-1 \times 10^{11}/\text{cm}^2$.

As observed that increases of the dielectric constant, the channel conductance decrease due to the reduction of drain current. It decreases with an increase in drain voltage. Using the following formula the channel conductance can be calculated;

$$g_d = \frac{\Delta I_{DS}}{\Delta V_{DS}} \tag{12}$$

The channel conductance variation can be calculated by using the following formula;

$$\Delta g_d = g_{d(Ref.)} - g_{d(Bio)} \tag{13}$$

g_d Should be higher to achieve high biomolecule sensitivity. Fig.10(a) and (b) show the channel conductance for neutral and charged biomolecules. The channel conductance decreases with the increase in negative charge associated with a biomolecule. Reduction in g_d Indicate the enhancement of device resistance due to capacitive coupling of higher negative charge in the cavity. The relative change in the channel conductance Δg_d is shown in Fig.11 (a) and Fig.11(b) for neutral and charged biomolecules, respectively. The channel conductance variation increases on increasing dielectric of neutral bio-molecule. In the case of charged biomolecules, the negatively charged biomolecules will have high channel conductance variation.

3.1 **Threshold voltage variation**

The threshold voltage decreases on increasing the permittivity of the neutral biomolecules in the cavity. Threshold voltage generally is a sensing parameter. Fig.12(a)

depicts the effect of neutral bio-molecules on the threshold voltage. The threshold voltage shows a positive shift with the increase of dielectric of neutral biomolecules, as shown in Fig.12(a).

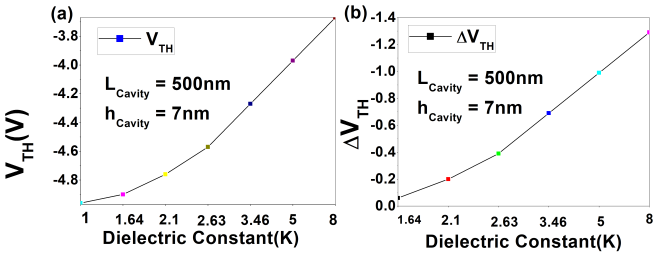

Fig. 12 (a) Threshold voltage and (b) shift in threshold voltage V_{th} for different neutral biomolecules.

The greater the variation, therefore greater the threshold sensitivity. The variation in V_{th} is depicted in Fig.12(b). The variation is higher for high k biomolecules. The threshold voltage variation can be calculated by using the following equations

$$\Delta V_{th} = V_{th(Ref.)} - V_{th(Bio)} \tag{14}$$

$$\Delta V_{th} = V_{th(Neutral)} - V_{th(charged\_Bio)} \tag{15}$$

Where, $V_{th(Ref.)}$ is the threshold voltage when the cavity is empty, $V_{th(Bio)}$is when the cavity is filled with a biomolecule, $V_{th(Neutral)}$is when no interface charge is applied and $V_{th(charged\_Bio)}$ is when the cavity is filled with charged biomolecules.

Figure 13(a) indicates that the threshold voltage decreases as the negative charge of biomolecules in the cavity region of the device increases, whereas threshold voltage increases when the positive charge of biomolecules in the cavity region of the device increases. Fig.13(b) indicates that the threshold variation will have a high positive value of variation when increases the positive charge of the biomolecule whereas a high negative value of threshold variation with an increase in the negative charge of the biomolecule. The dielectric of neutral and

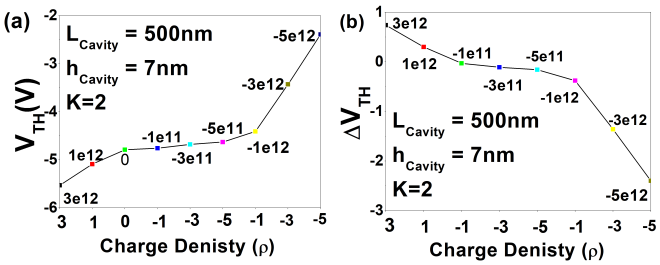

Fig. 13 (a) Threshold voltage and (b) shift in threshold voltage V_{th} for different charged biomolecules.

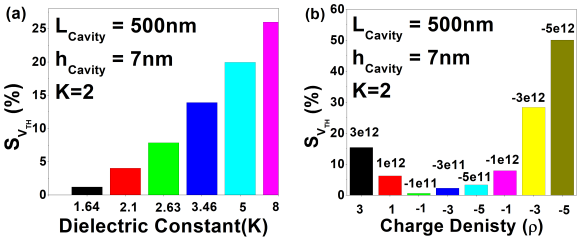

Fig. 14 Threshold voltage sensitivity for (a) neutral and (b) charged biomolecules at $L_{Cavity} = 500nm$

charged biomolecules influences the change in threshold voltage. The sensitivity was calculated using the following formula;

The V_{TH} sensitivity was calculated using the following formula;

$$S_{V_{th}} = \frac{V_{th(Ref.)} - V_{th(Bio)}}{V_{th(Ref.)}} \times 100 \tag{16}$$

In the case of neutral biomolecules, increasing the dielectric would increase sensitivity due to an increase in the threshold voltage variation, as seen in Fig.14(a). Fig.14(b) depicts the threshold voltage sensitivity due to the charge of biomolecules. Higher sensitivity is correlated with a higher negative charge, as shown in the figure. The highest sensitivity observed is for $-5\times10^{12}/cm^2$ in case of the charged biomolecule.

3.2 Impact of cavity length on device sensitivity

The effect of different cavity lengths on sensing is plotted and explained in this section. The cavity lengths considered in this analysis are 100nm, 300nm, and 500nm. To measure the sensitivity, the shift in threshold voltage and drain current variation are used. The change in threshold voltage for different cavity lengths is plotted for charged and neutral biomolecules.

3.2.1 ***Effect of cavity lengths on drain current variation for neutral and charged bio-molecules***

Figures 15(a) and (b) demonstrate the effect of cavity lengths on the drain current of neutral biomolecules. The maximum current variation was for K=8 obtained at 300nm cavity length for K=8 at VGS=0V is 22.9mA/mm. To measure the drain current variation, the following formula is used ;

$$\Delta I_{DS} = I_{DS(Ref.)} - I_{DS(Bio)} (A/mm) \tag{17}$$

where $I_{DS(Ref.)}$ is the current at K=1 when cavity is not occupied with neutral/charged biomolecule.

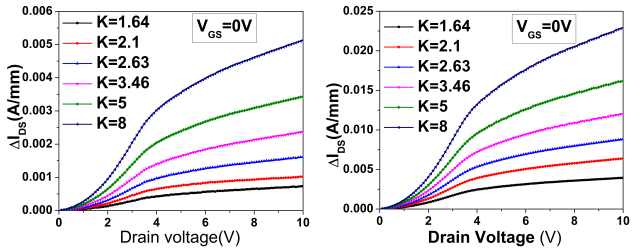

(a) (b)

Fig. 15 The drain current variation at V_{GS}=0V for (a) 100nm and (b) 300nm cavity lengths for neutral biomolecules

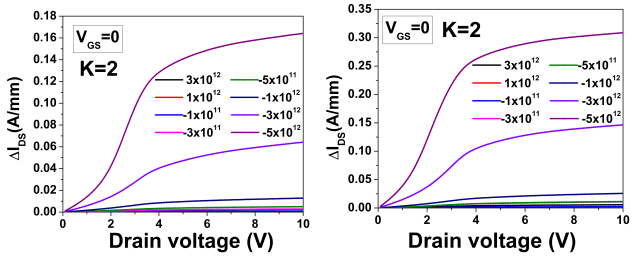

(a) (b)

Fig. 16 The drain current variation at V_{GS} = 0V for (a) 100nm and (b) 300nm cavity lengths for charged biomolecules

$I_{DS(Bio)}$ is the current when cavity is filled with neutral/charged biomolecules. The impact of cavity length on sensitivity for charged biomolecules is plotted in Fig.16 (a) and (b). The variation is high for 500nm cavity length due to the higher surface-to-volume ratio.

3.2.2 ***Impact of cavity length on Drain current sensitivity***

For various cavity lengths, the drain current sensitivity is calculated at V_{DS}=1V. The plots of sensitivity for The plots of sensitivity for 100nm, 300nm, and 500nm cavity lengths are shown in Fig.17 (a) and (b), respectively.

The drain current sensitivity for neutral and charged biomolecules is calculated using the following equation; ;

$$S_{I_{DS}} = \frac{I_{DS(Ref.)} - I_{DS(Bio)}}{I_{DS(Ref.)}} \times 100 \tag{18}$$

Where $I_{DS(Ref.)}$ is the current value when the cavity is empty, $I_{DS(Bio)}$ is when the cavity has some biomolecule. As on increasing dielectric and cavity length of neutral and charged biomolecules, the sensitivity also increases. By increasing cavity length, the sensitivity will increase due to the increases in surface area for biomolecule.

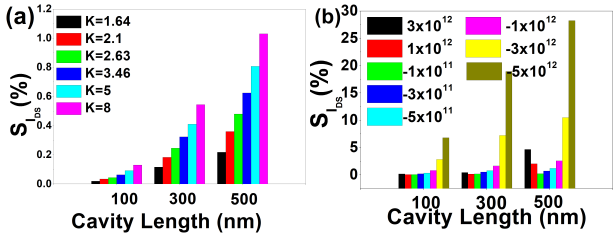

Fig. 17 Drain current sensitivity for (a) neutral and (b) charged biomolecules

More negative charged biomolecule indicate more variation in drain current that will lead to higher sensitivity. These plots show the pure effect of biomolecules on device sensitivity at V_{GS} = 0V.

3.2.3 ***Impact of cavity length on threshold voltage sensitivity***

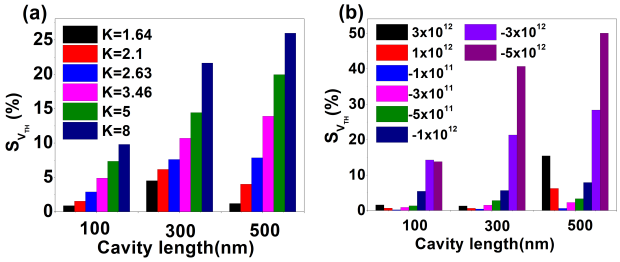

Fig. 18 Threshold voltage sensitivity of (a) neutral and (b)charged biomolecule at different cavity lengths

The device's sensitivity for neutral and charged biomolecules is calculated due to threshold voltage variation using Eq.16. The change in sensitivity is due to the shift of threshold voltage for different neutral/charged biomolecules. Fig.18 (a) and (b) show the sensitivity for neutral and charged biomolecules, respectively. For neutral biomolecules, the maximum sensitivity for K=8 is 26%, whereas, for charged biomolecules, 51% for -5 $\times$ 10^{12}/cm^2. The sensitivity will increase as the cavity length increases. The sensitivity for high k biomolecule will be higher. In the case of charged biomolecules, the sensitivity is affected by both charge and dielectric. Fig.18 (b) shows the sensitivity plot for charged biomolecule at the constant value of dielectric (K=2). The graph depicts that the sensitivity of a particular biomolecule increase as the negative charge associated with it increases.

3.3 Impact of mole fraction of barrier layer

The polarization field in the device increases as the mole fraction increases. The polarization is caused by a lattice mismatch between the GaN and the barrier layer.

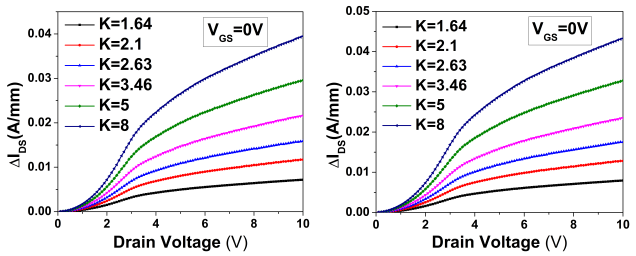

Fig. 19 The drain current variation at V_{GS} = 0V for neutral biomolecule at (a) x=0.22 and (b) x=0.25 value of mole fraction.

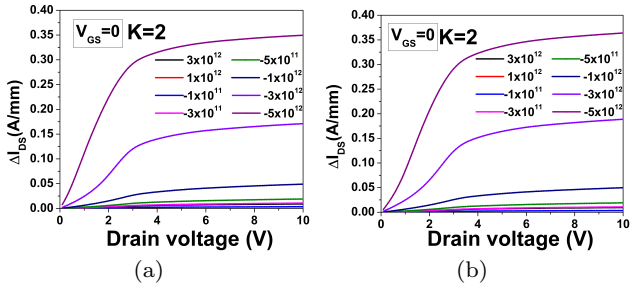

Fig. 20 The drain current variation at V_{GS} = 0V for charged biomolecules at (a) x=0.22 and (b) x=0.25 value of mole fraction.

With an increase in Al content in the barrier layer, the polarization fields increase. Due to the control on the conduction band discontinuity at heterojunction increase of mole fraction of barrier increases the drain current, which will allow high electron confinement in the channel. Different mole fraction values are considered here (x=0.22,0.25,0.30) to evaluate the mole fraction effect.

As an increase of mole fraction, the band-gap also increases. The higher the band gap exhibits higher stability of the device at high-temperature conditions. The higher band-gap was obtained at x=0.30. The band-gap can be calculated using the following equation for different mole fractions;

$$E_g(x) = x6.13 + (1-x)3.42 - x(1-x)eV \quad (19)$$

Where x is the value of mole fraction(x = 0.22, 0.25, 0.30). Where x is the value of mole fraction(x = 0.22, 0.25,0.30). The effect of mole fraction on drain current and the threshold voltage is reported in this section. Fig.19 (a) and (b) show the drain current variation due to mole fraction. The minimum current change is observed for Keratin at x = 0.22 is 36.59mA/mm V_{GS}=0V and maximum is 43.14mA/mm at V_{GS}=0V for Keratin at x=0.25. Increasing the biomolecule species also increases the variation in drain current. Fig.20 (a) and (b) depict the absolute variation in drain current for charged biomolecules. The higher the negative charge higher the variations in current.

3.3.1 ***Impact of mole fraction on Drain current and threshold voltage sensing***

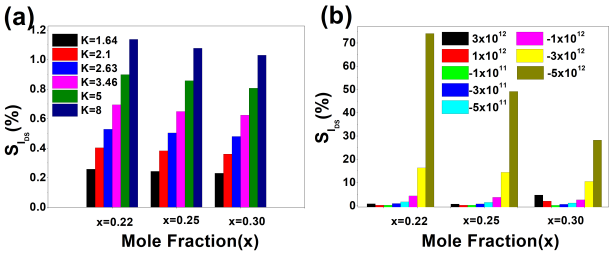

Fig. 21 Mole fraction effect on drain current sensitivity of (a) neutral biomolecules and (b) charged biomolecules.

Fig.21 (a) and (b) depict the sensitivity analysis of drain current for charged and neutral biomolecules, respectively. The variation of drain current is high for the mole fraction value of x=0.22. The maximum drain current sensitivity for charged biomolecules is 74.03% for $-5 \times 10^{12}/cm^2$ at x=0.22 and minimum is 28.24% at x=0.30. The threshold voltage sensitivity is depicted in fig.22 (a) and (b), respectively. The maximum threshold sensitivity obtained is 68% for $-5 \times 10^{12}/cm^2$at x=0.22 and minimum is 50% at x=0.30.

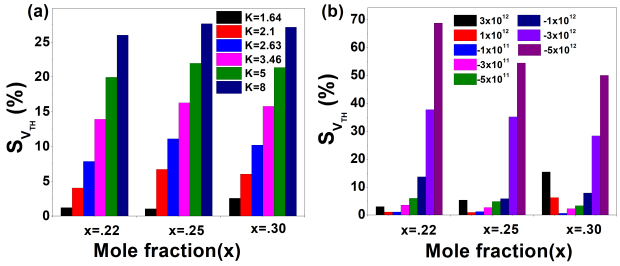

Fig. 22 Threshold voltage sensing due to different mole fraction for (a) neutral biomolecules and (b) charged biomolecules.

3.4 **Comparative analysis**

Table (2) presents the comparison between the previously reported work and the present study. The drain current variation obtained in the present work is higher than the previous for neutral bio-molecules, indicating higher sensitivity. The present study reports that the drain current sensitivity for Keratin is 99.9, which is

57.8% greater than reported [27]. The threshold voltage sensitivity is reported in this work is 26% which is 4% higher than reported [27].

Table 2 Comparison of drain current and threshold voltage variation for neutral Bio-molecules

Dielectric	ΔI_{DS}(mA/mm)	ΔI_{DS}	ΔV_{th}(V)	ΔV_{th}
1.64	8.90	$374.70\mu A/mm$[19]	0.06	47-160mV[19]
2.10	14.90	0.0538mA/mm[30]	0.20	0.11V[30]
2.63	19.90		0.39	
3.46	27.20		0.69	
5.00	37.40		0.99	0.45V[30]
8.00	50.70		1.29	

The maximum threshold voltage variation observed for charged biomolecules is 2.40V, more elevated than the previously reported work (0.1-0.5)[27].

4 CONCLUSIONS

With a Nano-cavity under the gate area, AlGaN/AlN/GaN MOS-HEMT is proposed. The threshold voltage and drain current sensitivity were obtained for neutral biomolecules in the range of 0.06-1.29mv and 8.9-50.7mA/mm. The analyzed voltage shift for DNA charge is up to 0.38V, and the current variation is 43.02mA/mm. The maximum threshold sensitivity obtained is 26% for keratin and 50.10% for charged biomolecules, respectively. The influence of cavity length and mole fraction is configured to determine the device's efficiency. Threshold voltage sensing, change in drain current, and channel conductance is the sensor performance parameters. The study indicates that MOS-HEMT derived on the cavity makes it suitable for applications of bio-sensing. It demonstrates a high sensitivity to neutral and charged biomolecules of all kinds.

Acknowledgments

The authors would like to the Department of Electronics and Communication Engineering, Malaviya National Institute of Technology for providing necessary support for carrying out the simulation work.

Author's Contributions

This work was proposed and done by Ritu Poonia (Author 1). Aasif Mohammad Bhat provided the necessary support regarding simulations and data interpretation. C. Periasamy and Chitrakant Sahu supervised the work and made important discussions and modifications to the final manuscript.

Funding

The authors have not received any funding for this work.

Data Availability

There are no linked research data sets for this submission.

Conflict of interest

The authors declare that they have no conflict of interest.

Ethical Approval

All procedures performed in studies involving human participants were in accordance with the ethical standards of the institutional and/or national research committee and with the 1964 Helsinki declaration and its later amendments or comparable ethical standards.

Informed Consent

Informed consent was obtained from all individual participants included in the study.

Consent to Participates

NA

Consent to Publication

NA

References

1. R. Kirste, N. Rohrbaugh, I. Bryan, Z. Bryan, R. Collazo, A. Ivanisevic, Annual Review of Analytical Chemistry **8**, 149 (2015)
2. L. Yang, B. Duan, Z. Dong, Y. Wang, Y. Yang, Technical Review pp. 1–12 (2019)
3. G. Chung, T. Vuong, H. Kim, Results in Physics **12**, 83 (2019)
4. A. Varghese, C. Periasamy, L. Bhargava, S.B. Dolmanan, S. Tripathy, IEEE Sensors Letters **3**(4), 1 (2019)
5. H.Y. Liu, W.C. Hsu, W.F. Chen, C.W. Lin, Y.Y. Li, C.S. Lee, W.C. Sun, S.Y. Wei, S.M. Yu, IEEE Sensors Journal **16**(10), 3514 (2016)
6. L. Wang, L. Li, T. Zhang, X. Liu, J.P. Ao, Applied Surface Science **427**, 1199 (2018)

7. A.M. Bhat, N. Shafi, C. Sahu, C. Periasamy, IEEE Sensors Journal **21**(18), 19753 (2021). DOI 10.1109/JSEN.2021.3100475
8. F.S. Tulip, E. Eteshola, S. Desai, S. Mostafa, S. Roopa, B. Evans, S.K. Islam, IEEE transactions on nanobioscience **13**(2), 138 (2014)
9. C.H. Kim, C. Jung, H.G. Park, Y.K. Choi, Biochip J **2**(2), 127 (2008)
10. P.P.K. Reddy, S.B. Lakshmi, L. Arivazhgan, J.R. Kumar, D. Nirmal, in *IOP Conference Series: Materials Science and Engineering*, vol. 872 (IOP Publishing, 2020), vol. 872, p. 012048
11. B. Kang, H. Wang, F. Ren, S. Pearton, Journal of applied physics **104**(3), 8 (2008)
12. J.d. Li, J.j. Cheng, B. Miao, X.w. Wei, J. Xie, J.c. Zhang, Z.q. Zhang, D.m. Wu, Journal of Micromechanics and Microengineering **24**(7), 075023 (2014)
13. H.F. Huq, H. Trevino II, J. Castillo, Journal of Modern Physics **7**(13), 1712 (2016)
14. A. Varghese, C. Periasamy, L. Bhargava, IEEE Sensors Journal **18**(23), 9595 (2018)
15. S.A. Eliza, R. Olah, A.K. Dutta, Nanoscience and Nanotechnology Letters **2**(2), 139 (2010)
16. H.H. Lee, M. Bae, S.H. Jo, J.K. Shin, D.H. Son, C.H. Won, J.H. Lee, Sensors and Actuators B: Chemical **234**, 316 (2016)
17. I. Sarangadharan, A. Regmi, Y.W. Chen, C.P. Hsu, P.c. Chen, W.H. Chang, G.Y. Lee, J.I. Chyi, S.C. Shiesh, G.B. Lee, et al., Biosensors and Bioelectronics **100**, 282 (2018)
18. J. Yang, P. Carey IV, F. Ren, Y.L. Wang, M.L. Good, S. Jang, M.A. Mastro, S. Pearton, Applied Physics Letters **111**(20), 202104 (2017)
19. S. Mishra, K. Jena, Journal of the Korean Physical Society **74**(4), 349 (2019)
20. N. Sharma, N. Chaturvedi, IETE Technical Review **33**(1), 34 (2016)
21. N.M. Shrestha, Y. Li, E.Y. Chang, Japanese Journal of Applied Physics **53**(4S), 04EF08 (2014)
22. O. Ambacher, J. Smart, J. Shealy, N. Weimann, K. Chu, M. Murphy, W. Schaff, L. Eastman, R. Dimitrov, L. Wittmer, et al., Journal of applied physics **85**(6), 3222 (1999)
23. S. Jiang, Y. Cai, P. Feng, S. Shen, X. Zhao, P. Fletcher, V. Esendag, K.B. Lee, T. Wang, ACS Applied Materials & Interfaces **12**(11), 12949 (2020). DOI 10.1021/acsami.9b19697. PMID: 32090550
24. P. Pal, Y. Pratap, M. Gupta, S. Kabra, IEEE Sensors Journal **19**(2), 587 (2018)
25. N. Shafi, C. Sahu, C. Periasamy, Superlattices and Microstructures **120**, 75 (2018)
26. A. Paliwal, M. Tomar, V. Gupta, Journal of Applied Physics **116**(2), 023109 (2014)
27. P. Pal, Y. Pratap, M. Gupta, S. Kabra, H.D. Sehgal, in *2020 5th International Conference on Devices, Circuits and Systems (ICDCS)* (IEEE, 2020), pp. 203–206
28. F. Bibi, M. Villain, C. Guillaume, B. Sorli, N. Gontard, Sensors **16**(8), 1232 (2016)
29. H.H. Bragulla, D.G. Homberger, Journal of anatomy **214**(4), 516 (2009)
30. Y. Pratap, M. Kumar, S. Kabra, S. Haldar, R. Gupta, M. Gupta, Journal of Computational Electronics **17**(1), 288 (2018)